

Enhancing efficiency and power of quantum-dots resonant tunneling thermoelectrics in three-terminal geometry by cooperative effects

Jian-Hua Jiang*

*Department of Physics, University of Toronto, Toronto, Ontario, M5S 1A7 Canada and
Center for Phononics and Thermal Energy Science,*

School of Physical Science and Engineering, Tongji University, Shanghai, 200092 China

(Dated: July 6, 2015)

We propose a scheme of multilayer thermoelectric engine where *one* electric current is coupled to *two* temperature gradients in three-terminal geometry. This is realized by resonant tunneling through quantum dots embedded in two thermal and electrical resisting polymer matrix layers between highly conducting semiconductor layers. There are two thermoelectric effects, one of which is pertaining to inelastic transport processes (if energies of quantum dots in the two layers are different) while the other exists also for elastic transport processes. These two correspond to the transverse and longitudinal thermoelectric effects respectively and are associated with different temperature gradients. We show that cooperation between the two thermoelectric effects leads to markedly improved figure of merit and power factor which is confirmed by numerical calculation using material parameters. Such enhancement is robust against phonon heat conduction and energy level broadening. Therefore we demonstrated cooperative effect as an additional way to effectively improve performance of thermoelectrics in three-terminal geometry.

PACS numbers: 73.63.-b, 85.80.Fi, 85.35.-p, 84.60.Rb

I. INTRODUCTION

Harvesting usable energy from wasted heat using thermoelectrics has been attracting a lot of research interest.¹ Much efforts have been devoted to bulk materials, making them mature thermoelectric systems that are already useful in industrial technologies.^{2,3} Recently there is a trend of incorporating nanostructures to further improve the performance of thermoelectric materials.⁴⁻⁶ Successful examples have been achieved in many materials/structures along this direction.⁴⁻⁶ Theoretical studies have demonstrated that the thermoelectric properties of individual nanostructures can be much better than the bulk.⁷⁻¹⁰ Experimental efforts have pushed forward the measurements of thermoelectric properties of individual nanostructures.^{11,12} There are also studies trying to fill the gaps between the thermoelectric properties of individual nanostructures and their assemblies⁴⁻⁶ as well as attempts to improve thermoelectric performance by tuning the shape and organization patterns of nanostructures.¹³

In addition to material and structural aspects, geometry also plays an important role in thermoelectric applications. For example, transverse thermoelectrics¹⁴ take advantages of accumulating temperature difference in one direction while generating electric current in the perpendicular direction. Geometric separation of the electric and heat flows facilitates special functions. For example, thermoelectric cooling and engine can be realized using a single type of carrier doping (i.e., without serial connection between *n*- and *p*-type thermoelectric components) via transverse thermoelectric effect.¹⁴ Recently a related, but different, thermoelectric effect is found in mesoscopic thermoelectrics in three-terminal geometry.¹⁵⁻²⁸ Researches in this direction is pioneered by the theory

of Edwards *et al.*²⁹ and the later experiments.³⁰ The underlying physics is illustrated in Fig. 1 (see also Ref. 19): excess population of phonons can induce an electric current during inelastic transport processes. Heat and electric flows are geometrically separated since heat is carried by the phonons flowing from/into the phonon bath. This picture can be generalized to inelastic transport processes assisted by other elementary excitations, such as photons²⁰, electron-hole excitations^{17,18} and magnons.²¹ Besides the quantum dots (QDs) can be replaced with any conductors given that the carrier energies at the left and right conductors are considerably different, which can be realized by two low-dimensional structures (e.g., quantum wells²⁸ or wires), or a barrier,²⁶ or a band gap.²⁵

Microscopic analysis^{15,17-21,24-28} indicates that the performance of each individual nano-scale three-terminal thermoelectric (3T-TE) device is promising. Experiments have demonstrated the effectiveness of 3T-TE cooling at submicron scale.³⁰ In this work we focus on 3T-TE systems based on the structure illustrated in Fig. 2. This structure was initially proposed by Edwards *et al.*²⁹ and later explored experimentally in Ref. 30 for cooling of electrons at cryogenic temperature. Recently Jordan *et al.* extend the idea to thermoelectric engine with layered self-assembled QDs where considerable electrical current density could be obtained due to contributions from many parallel quantum tunneling channels²⁴. This proposal significantly improve the potential for thermoelectric energy harvesting of the original idea (An extended idea of replacing the QD layers by quantum wells is presented in Ref. 28). Here we exploit the same structure of Jordan *et al.* to study cooperative effects between the longitudinal and transverse thermoelectric powers.

In Fig. 2(a) the electronic cavity, as well as the source and the drain, are highly conducting layers made of

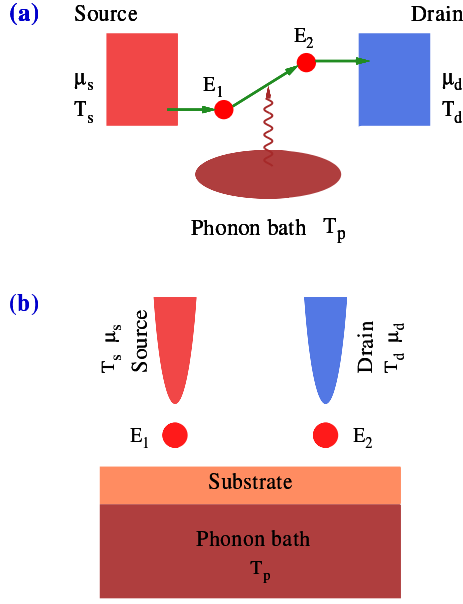


FIG. 1. (Color online) Illustration of a three-terminal thermoelectric system (studied in Ref. 19). (a) An electron first tunnels from the source to the quantum dot (represented by a red dot) with energy E_1 and then hops to the other quantum dot with energy E_2 by absorbing a phonon from the phonon bath. After that the electron tunnels into the drain electrode. The tunneling processes are elastic, while the hopping between quantum dots must be assisted by a phonon with energy $E_2 - E_1 > 0$. The temperatures of the source, drain and phonon bath are T_s , T_d , and T_p , while the electrochemical potentials of the source and drain are μ_s and μ_d , respectively. When the phonon bath has the highest temperature among the three reservoirs, excess number of phonons prefer phonon absorption processes and hence induces an electric current from the source to the drain. (b) In realistic situations the phonon bath is connected with the (insulating) substrate supporting the quantum dots while the two electrodes are suspended to be isolated from the phonon bath.

heavily-doped semiconductors (e.g., heavily-doped silicon or GaAs). In between those layers, there are two highly resisting layers with high thermal and electrical resistance. Each of the resisting layer is embedded with a QD through which electrons can tunnel between the cavity and the electrodes. The resonant tunneling through QDs are responsible for the transport. The energy levels in the left and right QDs are E_1 and E_2 , respectively. When $E_1 \neq E_2$, an electron transmitting from the source to the drain takes a finite amount of energy, $E_2 - E_1$, from the cavity. To reach steady states the cavity must exchange energy with the phonon bath [see Fig. 2(b)]. The transverse thermoelectric effect is manifested as the fact that an electric current drives a heat current from the phonon bath [see Fig. 2(b)], and vice versa.

Following Ref. 24, the scheme to assemble the nano-scale devices into a macroscopic device is straightforward: 2D arrays of QDs can be placed in the resisting layers [see Fig. 2(c)]. This can be realized by self-assembled QDs

grown on the surface of semiconductors,³¹ or as we proposed here, core-shell QDs embedded in (undoped) polymers with low thermal and electrical conductance.^{32–35} In such an assembly scheme the total electric current is the sum of the electric currents in each nano-scale 3T-TE device (i.e., a pair of QDs). High power density can be prompted by high density of QDs which can reach $\sim 10^{11} \text{ cm}^{-2}$ for a single layer (about 1 nm thick).³¹

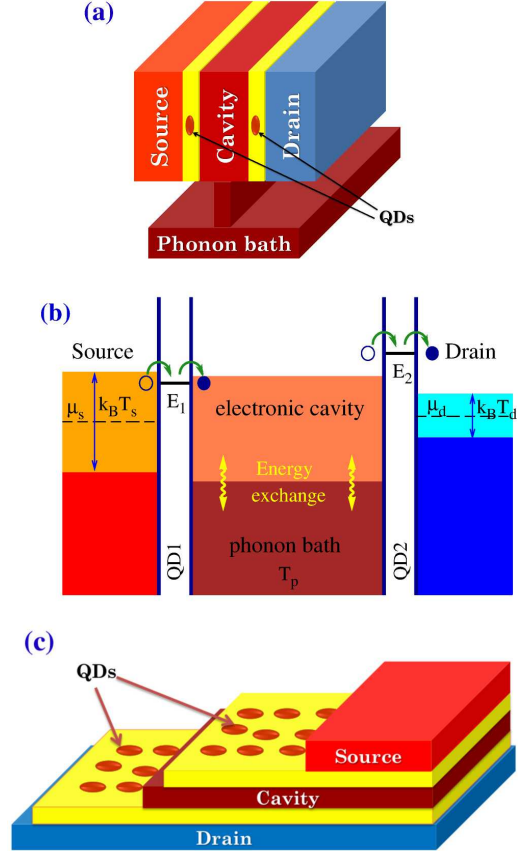


FIG. 2. (Color online) Illustration of the 3T-TE device studied in this work. (a) Schematic of a possible realistic set-up. The layered structure consists of three highly conducting regions: the source, cavity, and drain. In between them there are two highly resisting layers (yellow regions) with very low thermal and electrical conductance. A QD is embedded into each resisting layer to allow electrical and thermal conduction through it. The cavity is connected with a (insulating) phonon bath. The connection allows efficient energy exchange between them. (b) Illustration of the microscopic processes. Carrier distributions in the source and the drain are determined by the chemical potentials and temperatures. Electrons transmit through QDs via resonant tunneling. When energies of the two QDs, E_1 and E_2 , are different, energy exchange between the cavity and the phonon bath is necessary for the establishment of the steady state transport. (c) A scheme for building macroscopic devices where many QDs, forming 2D arrays, are embedded in the resisting layers.

To date all works on 3T-TE systems focus on exploiting the transverse thermoelectric effect. However, there is also a longitudinal thermoelectric effect in the system:

the temperature difference between the two electrodes can also induce an electric current. A full description of thermoelectric transport in 3T-TE systems is given by the phenomenological equation (similar equations were found in Refs. 16, 19, 23, and 25)

$$\begin{pmatrix} I \\ I_{Q1} \\ I_{Q2} \end{pmatrix} = \begin{pmatrix} G & L_1 & L_2 \\ L_1 & K_1 & K_{12} \\ L_2 & K_{12} & K_2 \end{pmatrix} \begin{pmatrix} V \\ \Delta T_1/T \\ \Delta T_2/T \end{pmatrix}, \quad (1)$$

where L_1 and L_2 represent the longitudinal and transverse thermoelectric effects, respectively. I_{Q1} and I_{Q2} stand for the heat currents leaving the source and the phonon bath, respectively. The two temperature differences are $\Delta T_1 = T_s - T_d$ and $\Delta T_2 = T_p - T_d$ with T_s , T_d , and T_p being the temperatures of the source, the drain, and the phonon bath, respectively.

In this work we show that, if both the longitudinal and transverse thermoelectric effects are exploited simultaneously, due to cooperation between the two, the efficiency and power can be considerably improved. The cooperative effect originates deeply from the nature of three-terminal thermoelectric systems: the two thermoelectric effects are correlated with each other, or in other words, the electrical current are *simultaneously* induced by the two *different* temperature gradients. Simplified geometric interpretation is that the electric currents induced by the two thermoelectric effects can be parallel or anti-parallel. In the former case the two effects add up constructively, leading to enhanced thermopower and efficiency. The phenomenon reflects the cooperative effect of two (or more) correlated thermoelectric effects which is referred to as the “cooperative thermoelectric effect”.

The cooperative thermoelectric effect is manifested in the proposed thermoelectric device. Using material parameters we calculate the thermoelectric transport coefficients as well as the figure of merit and power factor. It is found that both the figure of merit and the power factor are considerably improved by the cooperative thermoelectric effect. This enhancement is as effective for good thermoelectrics as that for bad thermoelectrics. In calculation we show that the enhancement induced cooperative effect changes only slightly when phonon heat conductivity or QD energy broadening is increased significantly. These results demonstrate that cooperative effect is an alternative way to improve the performance of thermoelectrics in three-terminal geometry effectively.

This paper is organized as follows: In Sec. II we establish thermoelectric transport of the 3T-TE systems from microscopic theory. In Sec. III we demonstrate the cooperative thermoelectric effect in a geometric way. In Sec. IV we calculate the thermoelectric transport coefficients as well as the figures of merit and power factors for the longitudinal, transverse, and cooperative thermoelectric effects for the 3T-TE systems using material parameters. We conclude in Sec. V. Studies in this work are focused on linear-response steady state transport. Interesting nonlinear effects³⁶ could be discussed in future works.

II. MICROSCOPIC THEORY OF THERMOELECTRIC TRANSPORT

In this section we develop a microscopic theory of 3T-TE transport, following the formalism of Jordan *et al.*²⁴ The system is a layered structure with thickness $L_{tot} = L_s + L_d + L_c + 2L_{qd}$ where L_s , L_d , L_c , and L_{qd} are the thickness of the source, the drain, the cavity, and the resisting layers, respectively. For realistic design, L_s , L_d , and L_c is about one hundred nanometers (nm), while L_{qd} is on the order of ten nm. The size of QDs is a few nm. The level spacing of the QDs, typically on the order of 100 meV for core-shell QDs (see Ref. 37), is much larger than $k_B T$. We suggest to fabricate serially connected unit structures [the structure in Fig. 2(a)] to scale the device up to a fully three-dimensional macroscopic device which can be implemented via layer-by-layer growth methods.

The Hamiltonian of the system is written as

$$H = H_s + H_d + H_c + H_{qd} + H_{int}, \quad (2)$$

where H_s , H_d , H_c , and H_{qd} are the Hamiltonian of the source, the drain, the cavity, and the QD, respectively. $H_\alpha = \sum_{\vec{k}} \varepsilon_{\vec{k}} c_{\vec{k},\alpha}^\dagger c_{\vec{k},\alpha}$, where $\alpha = s, d, c$ denotes the source, the drain, and the cavity, respectively. $\varepsilon_{\vec{k}} = \frac{\hbar^2 k^2}{2m^*}$ with m^* being the effective mass of the charge carrier.

$$H_{qd} = \sum_i E_i^{(\ell)} d_i^\dagger d_i + \sum_j E_j^{(r)} d_j^\dagger d_j, \quad (3)$$

where the index i and j numerate the QDs in the left (ℓ) and right (r) resisting layers, respectively. H_{int} describes hybridization of the QD states with the states in the source, drain, and cavity,

$$H_{int} = \sum_{\alpha=s,c} \sum_{\vec{k},i} V_{i,\alpha,\vec{k}}^{(\ell)} c_{\vec{k},\alpha}^\dagger d_i + \sum_{\alpha=d,c} \sum_{\vec{k},j} V_{j,\alpha,\vec{k}}^{(r)} c_{\vec{k},\alpha}^\dagger d_j + \text{H.c.} \quad (4)$$

The electric and thermal currents through the left resisting layer from the source to the cavity are given by³⁸

$$I_{e,\ell} = \frac{2e}{h} \int dE t_\ell(E) [f_s(E) - f_c(E)], \quad (5a)$$

$$I_{Q,\ell} = \frac{2}{h} \int dE (E - \mu) t_\ell(E) [f_s(E) - f_c(E)], \quad (5b)$$

respectively. The factor of two comes from the spin degeneracy of the carriers. e is the electronic charge. f_s and f_c are the carrier distribution functions of the source and the cavity, respectively. They are determined by the temperatures of the source T_s and the cavity T_c as well as by their electrochemical potentials μ_s and μ_c . Note that because the voltage and temperature gradients are mainly distributed at the two resisting layers, as a good approximation, one can assign uniform chemical potentials and temperatures to the source, drain, and cavity regions. The energy dependent transmission through QDs

is given by^{16,38} $t_\ell(E) = \sum_i t_i(E)$ with

$$t_i(E) = \frac{\hbar^2 \Gamma_{s,i}(E) \Gamma_{c,i}^{(\ell)}(E)}{(E - E_i^{(\ell)})^2 + \frac{\hbar^2}{4} \left(\Gamma_{s,i}(E) + \Gamma_{c,i}^{(\ell)}(E) \right)^2}, \quad (6)$$

where

$$\Gamma_{s,i}(E) = \frac{2\pi}{\hbar} \sum_{\vec{k}} |V_{i,s,\vec{k}}^{(\ell)}|^2 \delta(E - \varepsilon_{\vec{k}}), \quad (7a)$$

$$\Gamma_{c,i}^{(\ell)}(E) = \frac{2\pi}{\hbar} \sum_{\vec{k}} |V_{i,c,\vec{k}}^{(\ell)}|^2 \delta(E - \varepsilon_{\vec{k}}), \quad (7b)$$

are the energy-dependent tunneling rates from the QD i to the source and the cavity, respectively. The electric and thermal currents from the drain to the cavity can be obtained by the replacements: $i \rightarrow j$, $\ell \rightarrow r$, and $s \rightarrow d$. Introducing

$$G_\ell = \frac{2e^2}{\hbar k_B T} \int dE t_\ell(E) f(E) [1 - f(E)] \quad (8a)$$

$$L_\ell = \frac{2e}{\hbar k_B T} \int dE (E - \mu) t_\ell(E) f(E) [1 - f(E)] \quad (8b)$$

$$K_\ell = \frac{2}{\hbar k_B T} \int dE (E - \mu)^2 t_\ell(E) f(E) [1 - f(E)] \quad (8c)$$

with $f(E)$ being the equilibrium carrier distribution, in the linear-response regime one can rewrite Eq. (5) as

$$I_{e,\ell} = G_\ell (\mu_s - \mu_c) / e + L_\ell (T_s - T_c) / T, \quad (9a)$$

$$I_{Q,\ell} = L_\ell (\mu_s - \mu_c) / e + K_\ell (T_s - T_c) / T. \quad (9b)$$

Expressions for the currents from the drain to the cavity $I_{e,r}$ and $I_{Q,r}$ can be obtained from the above by the replacements $\ell \rightarrow r$ and $s \rightarrow d$.

Inelastic scatterings, such as the electron-phonon and electron-electron scatterings, are crucial for the establishment of steady states in the cavity. In the concerned temperature range, 300 ~ 500 K, those scatterings are quite efficient. The heat transfer between the phonon bath and the cavity can be made efficient by using materials with high thermal conductivity to connect them. Interface thermal resistance can be reduced if the cavity and the phonon bath are made of the same material. We assume the thermal conduction between the phonon bath and the cavity is efficient and the temperature gradient across them and within the cavity is considerably smaller than that across the two polymer layers. In this way the temperature of the cavity is very close to that of the phonon bath and one can approximate that $T_c = T_p$.^{19,25}

Energy conservation gives $I_{Q,\ell} + I_{Q,r} + I_{Q,t} + IV = 0$, where $I_{Q,t}$ is the heat current from the phonon bath to the cavity. Therefore there are only two independent heat currents.^{19,23} In Eq. (1) the two independent heat currents are chosen as $I_{Q1} = I_{Q,\ell}$ and $I_{Q2} = I_{Q,t}$. Charge conservation, $I_{e,\ell} + I_{e,r} = 0$, determines the electrochemical potential of the cavity

$$\mu_c = (G_\ell + G_r)^{-1} \left\{ G_\ell \mu_s + G_r \mu_d + eT^{-1} [L_\ell (T_s - T_p) + L_r (T_d - T_p)] \right\}. \quad (10)$$

Inserting the above into Eqs. (1) and (9) we obtain

$$G = (G_\ell^{-1} + G_r^{-1})^{-1}, \quad L_1 = G \frac{L_\ell}{G_\ell}, \quad (11a)$$

$$L_2 = G \left(\frac{L_r}{G_r} - \frac{L_\ell}{G_\ell} \right), \quad K_1 = K_\ell - \frac{L_\ell^2}{G_\ell + G_r}, \quad (11b)$$

$$K_{12} = \frac{L_\ell (L_\ell + L_r)}{G_\ell + G_r} - K_\ell, \quad (11c)$$

$$K_2 = K_\ell + K_r - \frac{(L_\ell + L_r)^2}{G_\ell + G_r}. \quad (11d)$$

To understand these results, we rewrite the transport coefficients in terms of average electronic energies, following Mahan and Sofo,⁹

$$L_1 = e^{-1} G \langle E - \mu \rangle_\ell, \quad L_2 = e^{-1} G (\langle E \rangle_r - \langle E \rangle_\ell), \quad (12a)$$

$$K_1 = \frac{L_1^2}{G} + K_{tl}, \quad K_{12} = \frac{L_1 L_2}{G} - K_{tl}, \quad (12b)$$

$$K_2 = \frac{L_2^2}{G} + K_{tl} + K_{tr}. \quad (12c)$$

where

$$K_{tl} = e^{-2} G_\ell \left[\langle (E - \mu)^2 \rangle_\ell - \langle E - \mu \rangle_\ell^2 \right], \quad (13a)$$

$$K_{tr} = e^{-2} G_r \left[\langle (E - \mu)^2 \rangle_r - \langle E - \mu \rangle_r^2 \right]. \quad (13b)$$

The average in the above is defined as

$$\langle E^n \rangle_\beta \equiv \frac{\int dE E^n G_\beta(E)}{\int dE G_\beta(E)} \quad (14)$$

with $G_\beta(E) = \frac{2e^2}{\hbar k_B T} t_\beta(E) f(E) [1 - f(E)]$, for $\beta = \ell, r$ and $n = 0, 1, 2$. $G_\ell = \int dE G_\ell(E)$ and $G_r = \int dE G_r(E)$. One readily notices from Eq. (13) that K_{tl} and K_{tr} must be non-negative.

For a macroscopic system with area A the electrical conductivity is $\sigma = Gl_u/A$ with $l_u = 2l_{qd} + l_c + (l_s + l_d)/2$ being the thickness of an unit structure [the structure in Fig. 2(a)]. Similarly the thermal conductivities are $\kappa_1 = K_1 l_u / (AT)$, $\kappa_2 = K_2 l_u / (AT)$, and $\kappa_{12} = K_{12} l_u / (AT)$. The longitudinal and transverse thermopowers are

$$S_1 \equiv \frac{L_1}{TG} = \frac{\langle E - \mu \rangle_\ell}{eT}, \quad S_2 \equiv \frac{L_2}{TG} = \frac{\langle E \rangle_r - \langle E \rangle_\ell}{eT}. \quad (15)$$

S_2 is proportional to the energy difference, reflecting that it is associated with the inelastic processes. In contrary S_1 remains finite when inelastic processes vanish.

The total entropy production of the system in the linear response regime is written as

$$\frac{dS}{dt} = \frac{1}{T} \left(IV + I_{Q1} \frac{\Delta T_1}{T} + I_{Q2} \frac{\Delta T_2}{T} \right). \quad (16)$$

The second law of thermodynamics, $\frac{dS}{dt} \geq 0$, requires that³⁹

$$GK_1 \geq L_1^2, \quad GK_2 \geq L_2^2, \quad K_1 K_2 \geq K_{12}^2, \quad (17)$$

as well as that the determinant of the 3×3 transport matrix in Eq. (1) to be non-negative. Those requirements are satisfied for the transport coefficients in Eq. (12) because $K_{tl}, K_{tr} \geq 0$.

III. COOPERATIVE EFFECT: A GEOMETRIC INTERPRETATION

We parametrize the two temperature differences as

$$\Delta T_1 \equiv \Delta T \cos \theta, \quad \Delta T_2 \equiv \Delta T \sin \theta. \quad (18)$$

The exergy efficiency (or the “second-law efficiency”, see Refs. 40 and 42) of the thermoelectric engine is^{40–42}

$$\phi = \frac{-IV}{I_{Q1}\Delta T_1/T + I_{Q2}\Delta T_2/T} \leq \phi_{max} = \frac{\sqrt{ZT+1}-1}{\sqrt{ZT+1}+1}.$$

The exergy efficiency (“second-law efficiency”) is defined by the output *free energy* divided by the input *free energy*.^{40–42} It has been widely used in the studies of energy conversion in chemical and biological systems since its invention about 60 years ago.⁴¹ Recently it was applied to thermoelectric systems³. According to Ref. 39 the rate of variation of free energy associated with a current is given by the product of the current and its conjugated thermodynamic force. Hence the denominator of the above equation consists of heat currents multiplied by temperature differences. It has been shown in Ref. 42 that the relation between the efficiency of $\eta = W/Q$ for heat engine (or $\eta = Q/W$ for refrigerator) and the second-law efficiency ϕ is that $\phi = \eta/\eta_C$ where η_C is the Carnot efficiency. Thus Ioffe’s figure of merit is also obtained starting from the second-law efficiency. At given θ the figure of merit is

$$ZT = \frac{\sigma S_{eff}^2 T}{\kappa_{eff} - \sigma S_{eff}^2 T} \quad (19)$$

is the figure of merit. Here $S_{eff} = S_1 \cos \theta + S_2 \sin \theta$ and $\kappa_{eff} = (K_1 \cos^2 \theta + 2K_{12} \sin \theta \cos \theta + K_2 \sin^2 \theta)l_u/(AT)$. Upon optimizing the output power of the thermoelectric engine, one obtains⁴³

$$W_{max} = \frac{1}{4}P(\Delta T)^2, \quad (20)$$

with the power factor

$$P = \sigma S_{eff}^2. \quad (21)$$

When $\theta = 0$ or π , Eqs. (19) and (21) give the well-known figure of merit and power factor for the longitudinal thermoelectric effect^{1,9}

$$Z_l T = \frac{\sigma S_1^2 T}{\kappa_1 - \sigma S_1^2 T}, \quad P_l = \sigma S_1^2. \quad (22)$$

The transverse thermoelectric figure of merit and power factor, i.e., $\theta = \pi/2$ or $3\pi/2$, are given by^{19,25}

$$Z_t T = \frac{\sigma S_2^2 T}{\kappa_2 - \sigma S_2^2 T}, \quad P_t = \sigma S_2^2. \quad (23)$$

Fig. 3(a) shows ZT versus the angle θ in a polar plot for a specific set of transport coefficients satisfying the thermodynamic bounds in (17). Remarkably for $0 < \theta < \pi/2$

and $\pi < \theta < 3\pi/2$, ZT is *greater* than both $Z_l T$ and $Z_t T$. To understand the underlying physics, we decompose the electric current into three parts $I = I_0 + I_1 + I_2$ with $I_0 \equiv GV$, $I_1 \equiv L_1 \Delta T_1/T$, and $I_2 \equiv L_2 \Delta T_2/T$. The two thermoelectric effects add up constructively when I_1 and I_2 have the same sign which takes place when $0 < \theta < \pi/2$ and $\pi < \theta < 3\pi/2$. Fig. 3(b) shows the power factor versus the angle θ . The power factor is also *larger* when the two currents I_1 and I_2 are in the same direction. The cooperation of the two thermoelectric effects thus leads to enhanced figure of merit and output power.

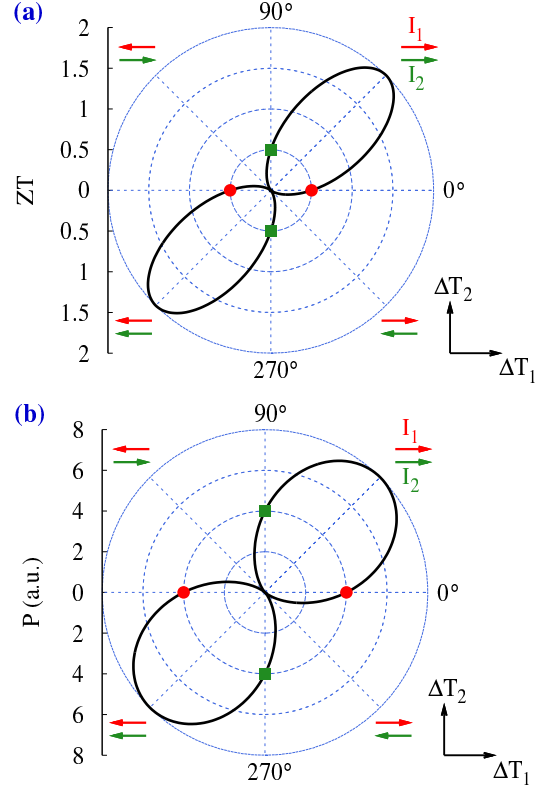


FIG. 3. (Color online) Polar plot of figure of merit ZT (a) and power factor P (b) [in arbitrary unit (a.u.)] versus angle θ . At $\theta = 0^\circ$ or 180° ZT and P recover the values for the longitudinal thermoelectric effect (red dots), while at $\theta = 90^\circ$ and 270° they go back to those of the transverse thermoelectric effect (green squares). The arrows in the I, II, III, IV quadrants label the direction of the currents $I_1 \equiv L_1 \Delta T_1/T$ (red arrows) and $I_2 \equiv L_2 \Delta T_2/T$ (green arrows). The transport coefficients are: $L_1 = L_2 = 2Gk_B T/e$, $K_1 = K_2 = 12G(k_B T/e)^2$, and $K_{12} = 0$. $I_0 \equiv GV$ (not shown) is reversed in III and IV quadrants for the operation of the thermoelectric engine.

One can maximize the figure of merit by tuning the angle θ . This is achieved at

$$\partial_\theta(ZT) = 0. \quad (24)$$

We find that the figure of merit is maximized at $\theta = \theta_M$

with

$$\tan(\theta_M) \equiv \frac{L_2 K_1 - L_1 K_{12}}{L_1 K_2 - L_2 K_{12}} = \frac{S_2 \kappa_1 - S_1 \kappa_{12}}{S_1 \kappa_2 - S_2 \kappa_{12}}. \quad (25)$$

After some algebraic calculation the maximum figure of merit is found to be

$$Z_M T = \frac{G(K_1 K_2 - K_{12}^2)}{D_M} - 1. \quad (26)$$

where $D_M = GK_1 K_2 - GK_{12}^2 - K_2 L_1^2 + 2L_1 K_{12} L_2 - K_1 L_2^2$ denotes the determinant of the 3×3 transport matrix in Eq. (1). $Z_M T$ is *greater* than both $Z_l T$ and $Z_t T$, unless the denominator or the numerator in Eq. (25) vanishes. Nevertheless it is guaranteed by Eqs. (12) and (13) that both the numerator and denominator in Eq. (25) is nonzero when the broadening of the quantum dot energy is finite.

One can also tune θ to maximize the power factor P which is achieved at

$$\partial_\theta P = 0. \quad (27)$$

The power factor is maximized at $\theta = \theta_m$ (in general $\theta_m \neq \theta_M$) with

$$\tan(\theta_m) \equiv \frac{L_2}{L_1} = \frac{S_2}{S_1}. \quad (28)$$

The maximum power factor

$$P_m = \sigma(S_1^2 + S_2^2) \quad (29)$$

is greater than both P_l and P_t unless S_1 or S_2 is zero. If θ_M is close to θ_m , both the figure of merit and the power factor can be improved by the cooperative effect simultaneously in certain range of θ .

The cooperative thermoelectric effect becomes particularly simple and vivid when $K_{12} = 0$, $K_1 = K_2 \equiv K$, $L_1 = L_2 \equiv L$, and $S \equiv L/(TG)$. In this special case the transport equation becomes

$$\begin{pmatrix} I \\ I_{Q1} \\ I_{Q2} \end{pmatrix} = \begin{pmatrix} G & L & L \\ L & K & 0 \\ L & 0 & K \end{pmatrix} \begin{pmatrix} V \\ \Delta T_1/T \\ \Delta T_2/T \end{pmatrix}. \quad (30)$$

We shall use the following combinations of temperature differences

$$\Delta T_a = \frac{\Delta T_1 + \Delta T_2}{\sqrt{2}}, \quad \Delta T_b = \frac{\Delta T_1 - \Delta T_2}{\sqrt{2}}. \quad (31)$$

The heat currents conjugate to the above forces are

$$I_{Qa} = \frac{I_{Q1} + I_{Q2}}{\sqrt{2}}, \quad I_{Qb} = \frac{I_{Q1} - I_{Q2}}{\sqrt{2}}. \quad (32)$$

The transport equation then becomes

$$\begin{pmatrix} I \\ I_{Qa} \\ I_{Qb} \end{pmatrix} = \begin{pmatrix} G & \sqrt{2}L & 0 \\ \sqrt{2}L & K & 0 \\ 0 & 0 & K \end{pmatrix} \begin{pmatrix} V \\ \Delta T_a/T \\ \Delta T_b/T \end{pmatrix}. \quad (33)$$

Consider conversion of heat I_{Qa} into work $-IV$ at $\Delta T_a \neq 0$ and $\Delta T_b = 0$. The figure of merit and power factor are

$$ZT = \frac{2L^2}{GK - 2L^2} = \frac{2\sigma S^2 T}{\kappa - 2\sigma S^2 T}, \quad P = 2\sigma S^2, \quad (34)$$

respectively, with $\kappa \equiv Kl_u/(AT)$. The above figure of merit and power factor are *greater* than those of the longitudinal and transverse thermoelectric effects which are

$$Z_l T = Z_t T = \frac{\sigma S^2 T}{\kappa - \sigma S^2 T}, \quad P_l = P_t = \sigma S^2. \quad (35)$$

IV. CALCULATION OF THERMOELECTRIC PERFORMANCE

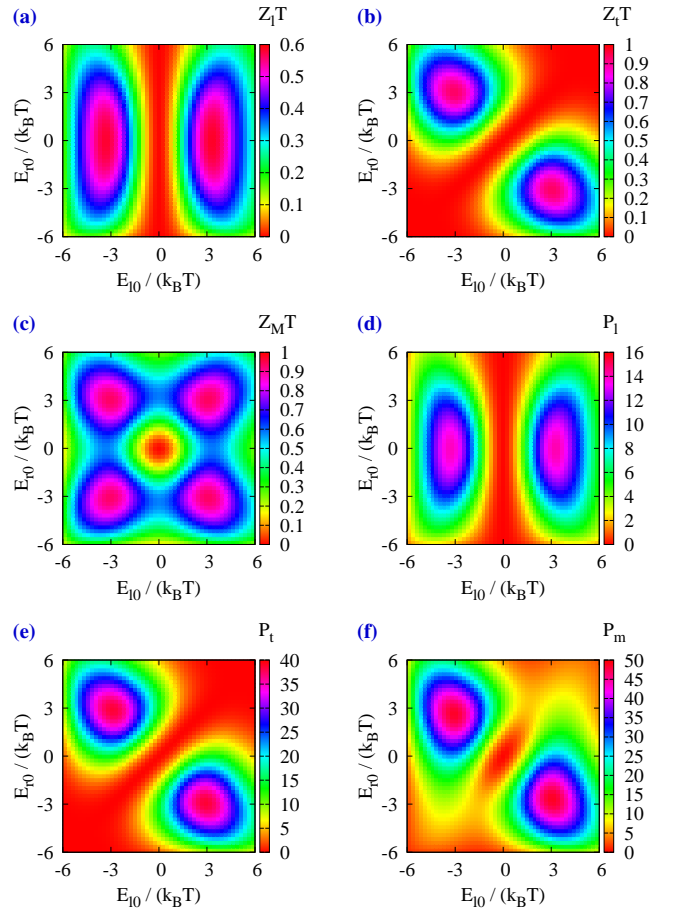


FIG. 4. (Color online) Figures of merit $Z_l T$ (a), $Z_t T$ (b), and $Z_M T$ (c), and power factors (in unit of $10^{-4} \text{ W m}^{-1} \text{ K}^{-2}$) P_l (d), P_t (e), and P_m (f) versus the QD energy E_{l0} and E_{r0} for $\Delta_{qd} = 20 \text{ meV}$ and $\kappa_p = 0.05 \text{ W m}^{-1} \text{ K}^{-1}$. The temperature is $T = 400 \text{ K}$, and the sheet density of QDs in each polymer layer (thickness 20 nm) is $4 \times 10^{12} \text{ cm}^{-2}$. QD tunneling linewidth is $\Gamma = 30 \text{ meV}$.

We now calculate the transport coefficients using material parameters. The robustness of the device performance is tested by including the randomness of QD

energy. Beside the transport mechanism described in Sec. II, there are other mechanisms conducting heat among reservoirs. The most important one is the heat conduction across the resisting layers by phonons. Polymers are good thermal insulators with heat conductivity $0.05 \sim 1 \text{ W m}^{-1} \text{ K}^{-1}$.^{32–34} Phonon thermal conductivity should be much reduced in the nano-scale thin films concerned here due to abundant scattering with the embedded QDs and interfaces.⁴ We take the phonon thermal conductivity as $\kappa_p = 0.05 \text{ W m}^{-1} \text{ K}^{-1}$ (e.g., bulk rayon³² has thermal conductivity of $0.05 \text{ W m}^{-1} \text{ K}^{-1}$). The thermal conductance across a resisting layer is $K_p = A\kappa_p T/l_{qd}$. Adding this contribution to the transport equation and using Eq. (12) leads to

$$\begin{aligned} K_1 &= \frac{L_1^2}{G} + K_{tl} + K_p, & K_{12} &= \frac{L_1 L_2}{G} - K_{tl} - K_p, \\ K_2 &= \frac{L_2^2}{G} + K_{tr} + K_{tl} + 2K_p. \end{aligned} \quad (36)$$

The variance of the QDs energy is several tens of meV as revealed by experiments.³¹ The thickness of the resisting layer is taken as $l_{qd} = 20 \text{ nm}$. The thickness of the source, the drain, and the cavity are all equal to 80 nm . High QD density, $2 \times 10^{13} \text{ cm}^{-2}$, has been realized in polymer matrices of thickness around 20 nm .³³ It is favorable to have more than one layer of QDs in each resisting layer to enable sufficient electron tunneling. Serial tunneling through several QDs may happen in the transmission across the resisting layers with many QDs.⁴⁴ We suggest to incorporate $\simeq 4 \times 10^{12} \text{ cm}^{-2}$ QDs into a 20 nm polymer layer which corresponds to a volume density of QDs as $\simeq 2 \times 10^{18} \text{ cm}^{-3}$ (average inter-dot distance $\simeq 8 \text{ nm}$). Taking into account of finite QD size, the inter-dot tunneling linewidth is $1 \sim 30 \text{ meV}$ depending on materials and structures which is taken as 30 meV here (see experimental measured value of 30 meV in Ref. 45). And we take $\Gamma \equiv \Gamma_{c,i}^{(\ell)}(E) = \Gamma_{c,j}^{(r)}(E) = \Gamma_{s,i}(E) = \Gamma_{d,j}(E) = 30 \text{ meV}$ ($\forall i, j, E$) as the QD tunneling linewidth used in calculating the tunneling rate. We shall study how the performance of the device varies with the variance and the mean value of the energy of QDs. The random QD energy in the left (right) resisting layer is modeled by a Gaussian distribution centered at $E_{\ell 0}$ (E_{r0}) with a variance Δ_{qd}^2 ,

$$g_\beta(E) = \frac{1}{\Delta_{qd}\sqrt{2\pi}} \exp\left[-\frac{(E - E_{\beta 0})^2}{2\Delta_{qd}^2}\right]. \quad (37)$$

with $\beta = \ell, r$. The QD energy and size can be controlled by various chemical³³ and physical³¹ methods during growth. We consider situations with temperature $T = 400 \text{ K}$. The energy zero is set to be the equilibrium chemical potential. The band edge of the semiconductor that constitutes the source, drain, and cavity layers is 200 meV below the chemical potential (a typical value for heavily-doped semiconductors). The electrical conductivity, thermopowers, and thermal conductivities are

calculated according to Eqs. (12), (13), and (14). Based on those transport coefficients we calculate the figures of merit and power factors, $Z_l T$, $Z_t T$, $Z_M T$ [Figs. 4(a), 4(b), and 4(c)], P_l , P_t , and P_m [Figs. 4(d), 4(e), and 4(f)].

Fig. 4 indicates that the figure of merit $Z_l T$ is optimized at the two points $E_{\ell 0} \simeq \pm 3k_B T$ with $E_{r0} = 0$, while $Z_t T$ is optimized at $E_{\ell 0} = -E_{r0} \simeq \pm 3k_B T$. These results, which are consistent with the results in Ref. 24, can be understood as the balance between large electrical conductivity, large thermopower, and small thermal conductivity in optimizing the figure of merit. The power factors, P_l and P_t , are optimized at parameters similar to those of $Z_l T$ and $Z_t T$, respectively. We find that when $Z_t T$ is optimized, $Z_M T$ is only slightly larger than $Z_t T$. For other situations, $Z_M T$ is considerably greater than both $Z_l T$ and $Z_t T$. Particularly near the two points $E_{\ell 0} = E_{r0} \simeq \pm 3k_B T$, the enhancement of figure of merit induced by cooperative effect is significant. For the power factor, cooperative effect always leads to considerable enhancement of power factor, unless when P_l or P_t are close to zero.

The above results reveal that cooperative effects can effectively improve the figure of merit and power factor for thermoelectrics in three-terminal geometry. Such improvement is especially useful for systems of which the electronic structure has not been fully optimized. Hence cooperative effects offer an additional way to improve the performance of thermoelectrics that are potentially useful for realistic systems. We also note that the largest figure of merit and power factor for the longitudinal thermoelectric effect are $Z_l T = 0.6$ and $P_l = 1.6 \times 10^{-3} \text{ W m}^{-1} \text{ K}^{-2}$ respectively, while the largest figure of merit and power factor for the transverse thermoelectric effect is $Z_t T = 1$ and $P_t = 4 \times 10^{-3} \text{ W m}^{-1} \text{ K}^{-2}$ respectively. This result confirms the conclusion in Refs. 19, 23–25, and 28 that the transverse thermoelectric effect in three-terminal geometry is of potential advantages.

In order to check the robustness of the effect in realistic situations we discuss the effect of the broadening of QD energy Δ_{qd} and the energy difference $E_{r0} - E_{\ell 0}$ for $E_{\ell 0} = 110 \text{ meV}$ ($\simeq 3k_B T$). Increase of the broadening of QD energy Δ_{qd} reduces the thermopower and increases the electronic heat conductivity. Therefore the figures of merit and power factors for the longitudinal, transverse, and cooperative thermoelectric effects are all reduced. From Fig. 5 one finds that considerably large figures of merit and power factors can still be obtained for broadening of QD energy up to 50 meV . In experiments the full width at half-maximum of photoluminescence spectra can be as small as 35 meV (i.e., the variance is 15 meV).³¹ Thus the proposed device is of potential application values. Finally in the above discussions only one energy level in each QD is considered. Careful calculation with higher energy levels (100 meV higher) included indicates that the figure of merit and the power factor are even larger [see Appendix].

We also plot the figures of merit and power factors for longitudinal, transverse, and cooperative thermoelectric

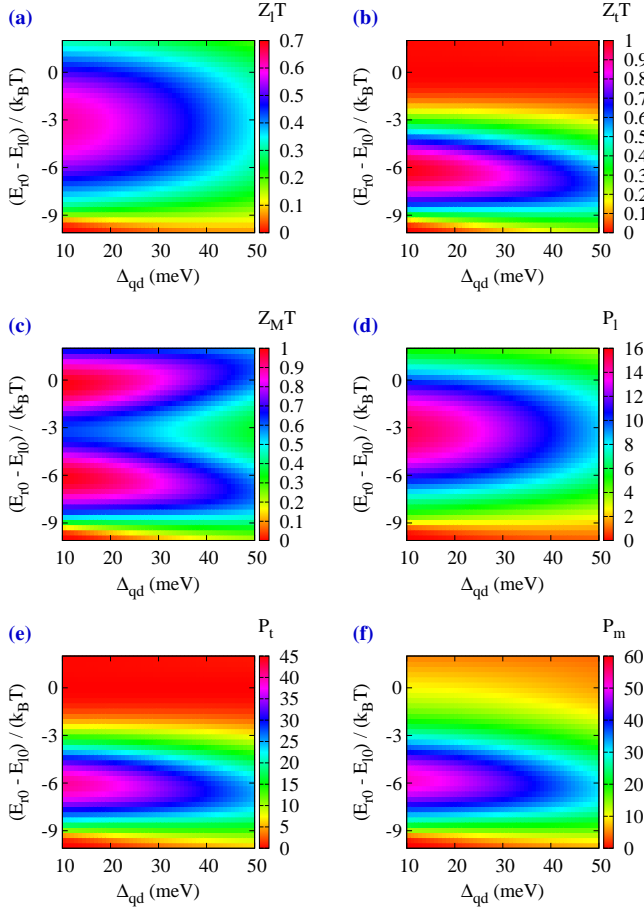


FIG. 5. (Color online) Figures of merit Z_lT (a), Z_tT (b), and Z_MT (c), and power factors (in unit of $10^{-4} \text{ W m}^{-1} \text{ K}^{-2}$) P_l (d), P_t (e), and P_m (f) versus the variance of the QDs energy Δ_{qd} and the difference of the mean values of QD energy in the two resisting layers $E_{r0} - E_{l0}$. Here E_{r0} is varying while $E_{l0} = 110 \text{ meV}$ ($\simeq 3k_B T$) is fixed. The temperature is $T = 400 \text{ K}$, $\kappa_p = 0.05 \text{ W m}^{-1} \text{ K}^{-1}$, and the sheet density of QDs in each polymer layer (of thickness 20 nm) is $4 \times 10^{12} \text{ cm}^{-2}$. QD tunneling linewidth is $\Gamma = 30 \text{ meV}$.

effects as functions of the tunneling linewidth of QDs Γ and the energy difference $E_{r0} - E_{l0}$ for $E_{l0} = 110 \text{ meV}$ ($\simeq 3k_B T$) in Fig. 6. Unlike the monotonic dependence on the variance of the QDs energy Δ_{qd} , the figures of merit and power factors first increases and then decreases with increasing Γ . This behavior is because at small Γ increase of Γ enhances electron tunneling and hence improves the electrical conductivity and the power factors. The enhancement of electron tunneling also improves electronic heat conductivity and reduces the effect of phonon heat conductivity on the figures of merit. Therefore, the figures of merit of the longitudinal, transverse, and cooperative thermoelectric effects are improved as well. However, the tunneling linewidth Γ also induces broadening of the energy of transported electron. When such broadening is comparable with or larger than the thermal energy $k_B T$, it considerably reduces the thermopowers and

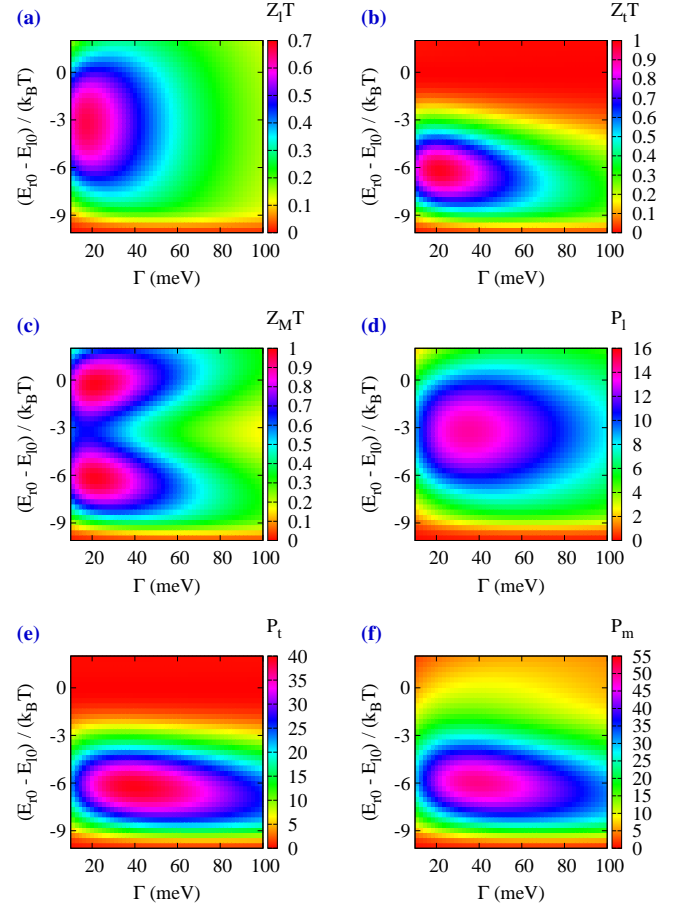


FIG. 6. (Color online) Figures of merit Z_lT (a), Z_tT (b), and Z_MT (c), and power factors (in unit of $10^{-4} \text{ W m}^{-1} \text{ K}^{-2}$) P_l (d), P_t (e), and P_m (f) versus the tunneling linewidth of QDs Γ and the difference of the mean values of QD energy in the two resisting layers $E_{r0} - E_{l0}$. Here E_{r0} is varying while $E_{l0} = 110 \text{ meV}$ ($\simeq 3k_B T$) is fixed. The temperature is $T = 400 \text{ K}$, $\kappa_p = 0.05 \text{ W m}^{-1} \text{ K}^{-1}$, and the sheet density of QDs in each polymer layer (of thickness 20 nm) is $4 \times 10^{12} \text{ cm}^{-2}$. The variance of the QDs energy is $\Delta_{qd} = 20 \text{ meV}$.

increases the electronic thermal conductivity, hence the power factors P_l , P_t , and P_m as well as the figures of merit Z_lT , Z_tT , and Z_MT are reduced. The optimal tunneling linewidths for Z_lT , Z_tT , and Z_MT are $\Gamma = 17.3, 21.4, 21.4 \text{ meV}$ respectively where the optimal figures of merit are $Z_lT = 0.668$, $Z_tT = 0.987$, and $Z_MT = 0.989$ respectively. Besides, the optimal tunneling linewidths for P_l , P_t , and P_m are $\Gamma = 34.5, 39.4, \text{ and } 38.6 \text{ meV}$ respectively where the optimal power factors are $P_l = 1.43 \times 10^{-3} \text{ W m}^{-1} \text{ K}^{-2}$, $P_t = 3.96 \times 10^{-3} \text{ W m}^{-1} \text{ K}^{-2}$, and $P_m = 5.02 \times 10^{-3} \text{ W m}^{-1} \text{ K}^{-2}$ respectively. The optimal figure of merit and power factor for the cooperative thermoelectric effect are larger than those of the transverse and longitudinal thermoelectric effects. This result is consistent with the proof in Sec. III that the figure of merit and the power factor of the cooperative thermoelectric effect is greater than or equal to those of the

longitudinal and transverse thermoelectric effects. Meanwhile the optimal performance of the transverse thermoelectric effect is also better than that of the longitudinal thermoelectric effect. Overall there are more parameter regions for the cooperative thermoelectric effect to have large values of the figure of merit and the power factor.

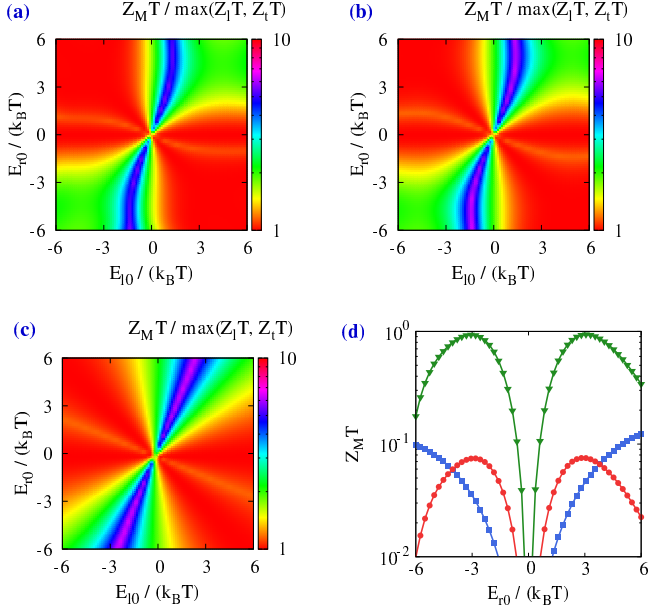


FIG. 7. (Color online) The enhancement of figure of merit $Z_M T / \max(Z_l T, Z_t T)$ versus the QD energy E_{l0} and E_{r0} for $\kappa_p = 0.05 \text{ W m}^{-1} \text{ K}^{-1}$ and $\Delta_{qd} = 20 \text{ meV}$ (a), as well as when the phonon heat conductivity is increased to $\kappa_p = 1 \text{ W m}^{-1} \text{ K}^{-1}$ or when the QD energy broadening is increased to $\Delta_{qd} = 150 \text{ meV}$ (c). In (d) figures of merit $Z_M T$ as a function of E_{r0} with $E_{l0} = E_{r0}$ is plotted for $\kappa_p = 0.05 \text{ W m}^{-1} \text{ K}^{-1}$ and $\Delta_{qd} = 20 \text{ meV}$ (curve with triangles), and for when the phonon heat conductivity is increased to $\kappa_p = 1 \text{ W m}^{-1} \text{ K}^{-1}$ (curve with dots) or when the QD energy broadening is increased to $\Delta_{qd} = 150 \text{ meV}$ (curve with squares). The temperature is $T = 400 \text{ K}$, and the sheet density of QDs in each polymer layer (thickness 20 nm) is $4 \times 10^{12} \text{ cm}^{-2}$. QD tunneling linewidth is $\Gamma = 30 \text{ meV}$.

Finally we demonstrate the robustness of the cooperative effects by examining the enhancement factor $Z_M T / \max(Z_l T, Z_t T)$ of thermoelectric figure of merit for $\kappa_p = 0.05 \text{ W m}^{-1} \text{ K}^{-1}$ and $\Delta_{qd} = 20 \text{ meV}$, as well as when the phonon parasitic heat conductivity is increased to $1 \text{ W m}^{-1} \text{ K}^{-1}$ or when the QD energy broadening is increased to $\Delta_{qd} = 150 \text{ meV}$. The results are plotted for different QD energies in Fig. 7. Considerable enhancement of figure of merit by cooperative effect is found around $E_{l0} \sim E_{r0}$ for a large portion of parameter region. Moreover, this enhancement by cooperative effect is still effective when the phonon heat conductivity is much enhanced or when the QD energy broadening is significantly increased. This result reveals that the cooperative effect remains effective in improving thermoelectric efficiency even in systems with small figure of merit induced by significant parasitic heat conductivity [see Fig. 7(d)].

V. CONCLUSION AND DISCUSSIONS

In summary we propose to enhance the thermoelectric efficiency and power by exploiting cooperative effects in three-terminal geometry. The three terminal geometry enables *one* electric current to couple with *two* temperature gradients with the help of inelastic transport processes. A scheme exploiting quantum-dots embedded in polymer matrices in multiple-layered structures is suggested to realize the principle. According to calculations based on material parameters, the figure of merit and power factor of the proposed structure are high, which indicates that layered resonant tunneling structures are potentially good thermoelectric systems.^{46,47} Marked improvements of figure of merit and power factor by the cooperative thermoelectric effect are obtained. Remarkably the enhancement of figure of merit and power factor induced by cooperative effects is robust to the parasitic phonon heat conductivity as well as quantum dots energy broadening. Hence we shown that cooperative effect offers an effective way to improve the figure of merit and power factor for three-terminal thermoelectric systems, particularly useful for systems of which the electronic structure has not been optimized. Study in this work indicates that exploiting geometric aspect, inelastic processes, and cooperative thermoelectric effects could provide alternative routes to high performance thermoelectrics.

ACKNOWLEDGEMENTS

We thank Baowen Li, Dvira Segal, Ming-Qi Weng, and Daoyong Chen for illuminating discussions. This work was partly supported by the NSERC and CIFAR of Canada, and the National Natural Science Foundation of China Grant No. 11334007.

APPENDIX: EFFECTS OF HIGHER LEVELS IN QDS ON THERMOELECTRIC PROPERTIES

We calculate the figures of merit $Z_l T$, $Z_t T$, and $Z_M T$ and power factors P_l , P_t , and P_m for the situation when there is another energy level of 100 meV higher than the original one in each QD for both the left and the right polymer layers. The results are plotted in Fig. 8. We assume that the tunneling rate of the higher level is the same as the lower one, i.e., $\Gamma = 30 \text{ meV}$. It is seen that the figures of merit as well as the power factors are all larger when the higher level is taken into account. Qualitatively, the results here is similar to those in Fig. 4 but with the center shifted toward lower energy for both E_{l0} and E_{r0} . This observation reveals that the main effect of the higher level is to enhance the electrical conductivity as well as the thermopower, which can be understood easily since a *higher* energy channel is introduced. However, introducing such a channel also increases the

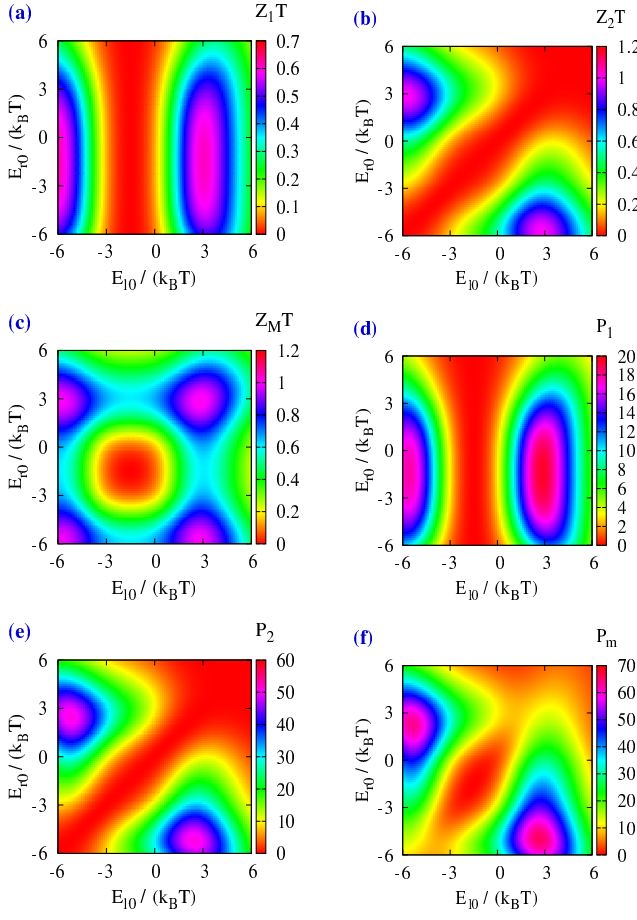


FIG. 8. (Color online) Figures of merit $Z_l T$ (a), $Z_t T$ (b), and $Z_M T$ (c), and power factors (in unit of $10^{-4} \text{ W m}^{-1} \text{ K}^{-2}$) P_l (d), P_t (e), and P_m (f) versus the QD energy E_{l0} and E_{r0} when there is another energy level of 100 meV higher than the original one and of the same tunneling rate in each QD for both the left and the right polymer layers. $\Delta_{qd} = 20 \text{ meV}$ and $\kappa_p = 0.05 \text{ W m}^{-1} \text{ K}^{-1}$. The temperature is $T = 400 \text{ K}$, and the sheet density of QDs in each polymer layer (thickness 20 nm) is $4 \times 10^{12} \text{ cm}^{-2}$. QD tunneling linewidth is $\Gamma = 30 \text{ meV}$.

thermal conductivity which normally would reduce the figure of merit.

To clarify the underlying mechanism, we plot the thermal conductivity κ_1 as a function of E_{r0} when $E_{l0} = E_{r0}$. In Fig. 9 we plot three different contributions of κ_1 : $\sigma S_1^2 T$, $[\sigma/(e^2 T)] [\langle (E - \mu)^2 \rangle_\ell - \langle E - \mu \rangle_\ell^2]$, and κ_p . The figure of merit $Z_l T$ is given by $Z_l T = \sigma S_1^2 T / (\kappa_1 - \sigma S_1^2 T)$. Indeed the thermal conductivity due to energy uncertainty $[\sigma/(e^2 T)] [\langle (E - \mu)^2 \rangle_\ell - \langle E - \mu \rangle_\ell^2]$ increases when higher level is introduced. However, in Fig. 9(a) (with the higher level) when $\sigma S_1^2 T$ reaches its maximum value, it is very close to the other two contributions. In comparison, in Fig. 9(b) (without the higher level) when $\sigma S_1^2 T$ reaches its maximum value, it is considerably smaller than the phonon heat conductivity κ_p . Therefore, the figure of

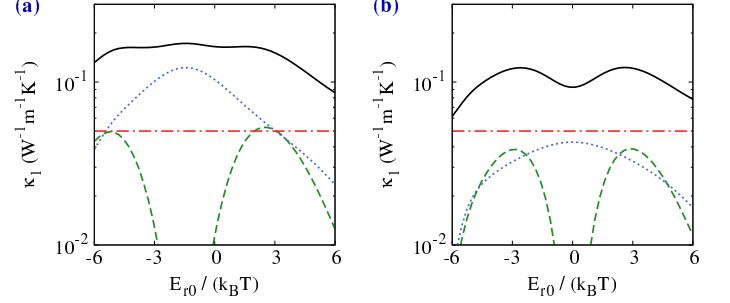


FIG. 9. (Color online) Heat conductivity κ_1 (black full curve) and its three contributions: $\sigma S_1^2 T$ (green dashed curve), $[\sigma/(e^2 T)] [\langle (E - \mu)^2 \rangle_\ell - \langle E - \mu \rangle_\ell^2]$ (blue dotted curve), and κ_p (red chained curve) as functions of $E_{r0} = E_{l0}$ for (a) with the higher level and (b) without the higher level. The higher level is 100 meV higher than the original level in each QD. $\Delta_{qd} = 20 \text{ meV}$ and $\kappa_p = 0.05 \text{ W m}^{-1} \text{ K}^{-1}$. The temperature is $T = 400 \text{ K}$, and the sheet density of QDs in each polymer layer (thickness 20 nm) is $4 \times 10^{12} \text{ cm}^{-2}$. QD tunneling linewidth is $\Gamma = 30 \text{ meV}$.

merit $Z_l T$ is enhanced when the higher level is taken into account. This particular feature is because in the case without the higher level, phonon heat conductivity predominately limits the figure of merit, rather than the variance of electronic energy.

* jianhua.jiang.phys@gmail.com

- ¹ T. C. Harman and J. M. Honig, *Thermoelectric and thermomagnetic effects and applications* (McGraw-Hill, New-York, 1967); H. J. Goldsmid, *Introduction to Thermoelectricity* (Springer, Heidelberg, 2009).
- ² G. J. Snyder and E. S. Toberer, *Nat. Mater.* **7**, 105 (2008); A. Shakouri, *Ann. Rev. of Mater. Res.* **41**, 399 (2011); T. M. Tritt, *Ann. Rev. of Mater. Res.* **41**, 433 (2011).
- ³ G. J. Snyder and T. S. Ursell, *Phys. Rev. Lett.* **91**, 148301 (2003).
- ⁴ R. Venkatasubramanian, *Phys. Rev. B* **61**, 3091 (2000); J.-K. Yu, S. Mitrovic, D. Tham, J. Varghese, and J. R. Heath,

- Nat. Nanotechnol.* **5**, 718 (2010); N. Nakpathomkun, H. Q. Xu, and H. Linke, *Phys. Rev. B* **82**, 235428 (2010); R. Venkatasubramanian, E. Siivola, T. Colpitts, and B. O'Quinn, *Nature* **413**, 597 (2001).
- ⁵ A. I. Boukai *et al.*, *Nature* **451**, 168 (2008); B. Poudel *et al.*, *Science* **320**, 634 (2008); P. Pichanusakorn and P. Bandaru, *Mater. Sci. Eng. R-Rep.* **67**, 19 (2010); A. J. Minnich, M. S. Dresselhaus, Z. F. Ren, and G. Chen, *Energy Environ. Sci.* **2**, 466 (2009); C. J. Vineis, A. Shakouri, A. Majumdar, and M. G. Kanatzidis, *Adv. Mater.* **22**, 3970 (2010); Z.-G. Chen, G. Han, L. Yang, L. Cheng, and J. Zou, *Prog. Nat. Prog. Nat. Sci.* **22**, 535 (2012); J.-F. Li,

- W.-S. Liu, L.-D. Zhao, and M. Zhou, *NPG Asia Mater.* **2**, 152 (2010).
- ⁶ M. S. Dresselhaus, G. Chen, M. Y. Tang, R. Yang, H. Lee, D. Wang, Z. Ren, J.-P. Fleurial, and P. Gogna, *Adv. Mater.* **19**, 1043 (2007).
 - ⁷ U. Sivan and Y. Imry, *Phys. Rev. B* **33**, 551 (1986).
 - ⁸ L. D. Hicks and M. S. Dresselhaus, *Phys. Rev. B* **47**, 12727 (1993); *ibid.*, **47**, 16631 (1993).
 - ⁹ G. D. Mahan and J. O. Sofo, *Proc. Natl. Acad. Sci. (USA)* **93**, 7436 (1996).
 - ¹⁰ T. E. Humphrey, R. Newbury, R. P. Taylor, and H. Linke, *Phys. Rev. Lett.* **89**, 116801 (2002); T. E. Humphrey and H. Linke, *Phys. Rev. Lett.* **94**, 096601 (2005).
 - ¹¹ P. Kim, L. Shi, A. Majumdar, and P. L. McEuen, *Phys. Rev. Lett.* **87**, 215502 (2001); D. Li, Y. Wu, P. Kim, L. Shi, P. Yang, and A. Majumdar, *Appl. Phys. Lett.* **83**, 2934 (2003); J. Hone, M. Whitney, C. Piskoti, and A. Zettl, *Phys. Rev. B* **59**, R2514 (1999); C. Yu, L. Shi, Z. Yao, D. Li, and A. Majumdar, *Nano Lett.* **5**, 1842 (2005).
 - ¹² F. Giazotto, T. T. Heikkilä, A. Luukanen, A. M. Savin, and J. P. Pekola, *Rev. Mod. Phys.* **78**, 217 (2006).
 - ¹³ *Thermoelectric Nanomaterials*, edited by K. Koumoto and T. Mori (Springer-Verlag, Berlin, 2013).
 - ¹⁴ S. L. Korylyuk *et al.*, *Sov. Phys. Semicond.* **7**, 502 (1973); V. P. Babin *et al.*, *Sov. Phys. Semicond.* **8**, 478 (1974); A. Kyarad and H. Lengfellner, *Appl. Phys. Lett.* **89**, 192103 (2006); C. Reitmaier, F. Walther, and H. Lengfellner, *Appl. Phys. A* **99**, 717 (2010); H. J. Goldsmid, *J. Electron. Mater.* **40**, 1254 (2011).
 - ¹⁵ S. Zippilli, G. Morigi, and A. Bachtold, *Phys. Rev. Lett.* **102**, 096804 (2009); B. Rutten, M. Esposito, and B. Cleuren, *Phys. Rev. B* **80**, 235122 (2009).
 - ¹⁶ O. Entin-Wohlman, Y. Imry, and A. Aharony, *Phys. Rev. B* **82**, 115314 (2010).
 - ¹⁷ R. Sánchez and M. Büttiker, *Phys. Rev. B* **83**, 085428 (2011); B. Sothmann, R. Sánchez, and A. N. Jordan, *arXiv:1406.5329*
 - ¹⁸ B. Sothmann, R. Sánchez, A. N. Jordan, and M. Büttiker, *Phys. Rev. B* **85**, 205301 (2012).
 - ¹⁹ J.-H. Jiang, O. Entin-Wohlman, and Y. Imry, *Phys. Rev. B* **85**, 075412 (2012).
 - ²⁰ T. Ruokola and T. Ojanen, *Phys. Rev. B* **86**, 035454 (2012).
 - ²¹ B. Sothmann and M. Büttiker, *Europhys. Lett.* **99**, 27001 (2012).
 - ²² L. Simine and D. Segal, *Phys. Chem. Chem. Phys.* **14**, 13820 (2012).
 - ²³ J.-H. Jiang, O. Entin-Wohlman, and Y. Imry, *Phys. Rev. B* **87**, 205420 (2013).
 - ²⁴ A. N. Jordan, B. Sothmann, R. Sánchez, and M. Büttiker, *Phys. Rev. B* **87**, 075312 (2013).
 - ²⁵ J.-H. Jiang, O. Entin-Wohlman, and Y. Imry, *New J. Phys.* **15**, 075021 (2013).
 - ²⁶ Y. Imry, O. Entin-Wohlman, and J. H. Jiang, *WO Patent* 2,013,035,100.
 - ²⁷ S. Juergens, F. Haupt, M. Moskalets, and J. Splettstoesser, *Phys. Rev. B* **87**, 245423 (2013); C. Bergenfeldt, P. Samuelsson, B. Sothmann, C. Flindt, and M. Büttiker, *Phys. Rev. Lett.* **112**, 076803 (2014); R. Bosisio, C. Gorini, G. Fleury, and J.-L. Pichard, *New J. Phys.* **16**, 095005 (2014); *ibid.*, *arXiv:1407.7020*.
 - ²⁸ B. Sothmann, R. Sánchez, A. N. Jordan, and M. Büttiker, *New J. Phys.* **15**, 095021 (2013).
 - ²⁹ H. L. Edwards, Q. Niu, and A. L. de Lozanne, *Appl. Phys. Lett.* **63**, 1815 (1993); H. L. Edwards, Q. Niu, G. A. Georgakis, and A. L. de Lozanne, *Phys. Rev. B* **52**, 5714 (1995).
 - ³⁰ J. R. Prance, C. G. Smith, J. P. Griffiths, S. J. Chorley, D. Anderson, G. A. C. Jones, I. Farrer, and D. A. Ritchie, *Phys. Rev. Lett.* **102**, 146602 (2009).
 - ³¹ S.-K. Park, J. Tatebayashi, and Y. Arakawa, *Appl. Phys. Lett.* **84**, 1877 (2004); S. Tonomura and K. Yamaguchi, *J. Appl. Phys.* **104**, 054909 (2008); M. Jo, T. Mano, Y. Sakuma, and K. Sakoda, *Appl. Phys. Lett.* **100**, 212113 (2012).
 - ³² Y. Yang, chap. 10 in *Physical Properties of Polymers Handbook*, edited by J. E. Mark (AIP Press, Woodbury, NY, 1996).
 - ³³ W. R. Algar and U. J. Krull, *Langmuir* **24**, 5514 (2008); S. Ishii, R. Ueji, S. Nakanishi, Y. Yoshida, H. Nagata, T. Itoh, M. Ishikawa, and V. Biju, *J. Photochem. Photobiol. A* **183**, 285 (2006).
 - ³⁴ K. Zhang, Y. Zhang, and S. Wang, *Scientific Reports* **3**, 3448 (2013).
 - ³⁵ The polymer electronic band gap should be considerably larger than the semiconductor band gap, so that the charge carriers in the doped semiconductor regions (i.e., the cavity, source, and drain) will not diffuse into the polymer resisting layers.
 - ³⁶ R. S. Whitney, *Phys. Rev. Lett.* **112**, 130601 (2014).
 - ³⁷ M. Gong, K. Duan, C.-F. Li, R. Magri, G. A. Narvaez, and L. He, *Phys. Rev. B* **77**, 045326 (2008); A. D. Lad and S. Mahamuni, *Phys. Rev. B* **78**, 125421 (2008).
 - ³⁸ H. Haug and A. P. Jauho, *Quantum Kinetics in Transport and Optics of Semiconductors*, (Springer, Berlin, 1996).
 - ³⁹ L. Onsager, *Phys. Rev.* **37**, 405 (1931); **38**, 2265 (1931).
 - ⁴⁰ Y. Demirel and S. I. Sandler, *J. Phys. Chem. B* **108**, 31 (2004).
 - ⁴¹ H. T. Odum and R. C. Pinkerton, *Am. Sci.* **43**, 331 (1955).
 - ⁴² J.-H. Jiang, *Phys. Rev. E* **90**, 042126 (2014).
 - ⁴³ C. Van den Broeck, *Phys. Rev. Lett.* **95**, 190602 (2005); M. Esposito, K. Lindenberg, and C. Van den Broeck, *Phys. Rev. Lett.* **102**, 130602 (2009).
 - ⁴⁴ S. A. Gurvitz, *Phys. Rev. B* **57**, 6602 (1998).
 - ⁴⁵ J. Berezovsky, O. Gywat, F. Meier, D. Battaglia, X. Peng, and D. D. Awschalom, *Nat. Phys.* **2**, 831 (2006).
 - ⁴⁶ K. Koumoto *et al.*, in *CRC thermoelectric handbook: Micro to Nano*, D. M. Rowe ed. (CRC press, USA, 2006).
 - ⁴⁷ A. Agarwal and B. Muralidharan, *Appl. Phys. Lett.* **105**, 013104 (2014).